Differentiation between copal and amber by their structure and thermal behaviour

M. Garcia-Valles[1] · A. Di Mariano[2] · P. Alfonso[3] · J. Noguès[1] · S. Martinez[1]

Abstract

The relationships between the polymerization related to structure and the composition of different types of natural resins were determined. Analyses were carried out by Fourier transform infrared spectroscopy (FTIR), differential thermal analysis–thermogravimetry (DTA-TG) and hot stage microscopy (HSM). Copal specimens were collected from the Mai-Ndombe Lake, Democratic Republic of Congo, and amber pieces that came from Bitterfeld, Germany, and from Kaliningrad, Russia. FTIR spectra of copal show a vibrational band at 1643 cm^{-1} (C=O stretching) attributed to communic acids, while amber shows a band at 1735 cm^{-1} associated with ester-group vibrations and a shoulder at about 3340 cm^{-1}, suggesting partial oxidization. DTA shows the main exothermic peak, related to the combustion, at 546–552 °C in amber and at 518 °C in copal. The derivative thermogravimetry (DTG) peaks vary in the different resin types; in amber, they occur at 333–335, 401–404 and 548–555 °C and are related to mass losses of 31, 26 and 39 mass%, respectively; copal peaks are at 394 and 507 °C, with mass losses of 71 and 27 mass%, respectively. In copal, hot stage microscopy (HSM) shows the start of sintering at 131 °C, followed by an expansion produced by the material decomposition and the generation of gases that cannot be released because of the material plastic behaviour. Finally, the increase in pressure produces an explosion that results in a lower viscosity of the liquid, which at this point can no longer support the internal pressure of gases. In amber samples, a smaller decrease in viscosity is observed and the start of sintering occurs at 150 °C with no significant change in their morphology.

Keywords Copal · Amber · Differential thermal analysis · Hot stage microscopy · Infrared and Raman spectroscopy

Introduction

Natural resins are semisolid amorphous organic hydrocarbon compounds secreted by plants. According to their degree of polymerization, they can be classified as amber or copal. Amber forms when resins from certain trees harden and gradually fossilize over long periods of time [1–3]. The resins hardening process starts when all volatile components are lost. At this point, resins become copal and with time, during burial of the host sediments, it undergoes further devolatilization, polymerization and oxidation processes that transform it into amber. Later, during burial with sediments they undergo to become amber [4].

The characterization of amber is important to distinguish it from false amber pieces, often appearing on the market. These can frequently be copal, a resin with a smaller degree of polymerization, or even synthetic resins, which may contain plants and/or insects to simulate amber [5]. Characterization of both amber and copal is useful not only for distinguishing cases of fraudulence but also for obtaining information about their provenance. To their assessment, studies are carried out on their chemical composition, molecular structure, the presence of minerals, and their thermal behaviour. These studies can provide relevant information about the origin and type of resins that make up valuable pieces [5]. The thermal behaviour of copal and amber provides evidence about their maturity degree [6]. Even though studies about the thermal behaviour of resins do already exist in the literature, they are still limited to

✉ M. Garcia-Valles
 maitegarciavalles@ub.edu

1   Departament de Mineralogia, Petrologia I Geologia Aplicada, Universitat de Barcelona, Barcelona, Spain

2   Geomechanics Group 1, CIMNE, Universitat Politècnica de Catalunya Barcelona Tech, Barcelona, Spain

3   Departament d'Enginyeria Minera, Industrial I TIC, Universitat Politècnica de Catalunya Barcelona Tech, Manresa, Spain

DTA-TG of samples [5, 7] or to differential scanning calorimetry (DSC) data [6, 8, 9].

Different types of amber are found in Europe; the largest deposits are located in the paleo-North Sea margin [10] and are known as Baltic amber or succinite. About 90% of the world's reserves of succinate are located in the Sambian Peninsula of the Kaliningrad Region, in Russia, where they have been mined since the Neolithic period [11]. They formed more than 40 million years ago in the middle Eocene [12] and contain a broad diversity of insects. A special characteristic of Baltic amber is its 3–8 mass% of succinic acids content [13].

Bitterfeld amber, which extends over the region of Saxony in Germany, has occasionally been considered as part of Baltic amber [14]; however, it is of more recent formation, belonging to the Late Oligocene [15] and/or Miocene. Baltic amber originates from the *Pinaceae* and *Sciadopityaceae* families [10], whereas Bitterfeld amber comes from the *Burseraceae* family [16]. Both resins are characterized by high amounts of succinic acid and terpenoid, but Baltic amber also contains diterpenoids which are absent in Bitterfeld amber [17].

Copal occurs in different locations around the world; the most known are those from Madagascar, Dominican Republic, Colombia, Indonesia, Mexico [18], New Zealand and several African countries. African copal has been extensively exploited, especially in the Congo area. All African copal derives from the *Fabaceae* family [19].

The purpose of the present research is to examine the main differences between copal and amber based on their spectroscopic analysis and their response to the application of heat. In addition to the DTA-TG, the rheological behaviour of some specimens was tested using hot stage microscopy (HSM). These analyses provide a good characterization of both resins.

Material and analytical methods

Samples

This study was carried out using five samples of copal from the Mai-Ndombe Lake, in the Democratic Republic of Congo, and four amber pieces belonging to the Escola de Gemmologia of the University of Barcelona coming from Bitterfeld, Germany, and from Yantarni (or Jantarnij), Kaliningrad, located in the Samland Peninsula, Russia.

Analytical methods

The colour of the samples was determined by spectral diffuse reflectance in the CIELAB colour space [20, 21]. The parameters were measured using a CM-700d Konica-Minolta spectrophotometer.

Tested samples were characterized by X-ray powder diffraction analysis (XRD). A small piece of material was cut from each sample, and a part of it was ground in an agate mortar. Analyses were performed using a PANalytical X'Pert PRO MPD alpha1 powder diffractometer in Bragg–Brentano $\theta/2\theta$ geometry of 240 mm of radius, CuKα_1 radiation ($\lambda = 1.5406$ Å) powered at 45 kV–40 mA, scanning range 4–100° with a 0.017° 2θ step size of 0.026° and measuring time of 100 s. Identification of phases was carried out using a PANalytical X'Pert HighScore software.

Microtextures were observed by scanning electron microscopy (SEM), using a Hitachi TM-1000 table top equipped with an energy-dispersive X-ray spectrometer (EDS). Observations were carried out in fractures and fragments of the resin pieces.

Fourier transform infrared (FTIR) spectra were obtained using a PerkinElmer System 2000 FTIR spectrometer. Vibrational spectra were recorded, in the 400–4000 cm^{-1} range, after 32 scans with a resolution of 4 cm^{-1}. Raman spectra were obtained using a micro-Raman spectrometer HORIBA Jobin Yvon LabRam HR 800, equipped with an Olympus BXFM optical microscope (10×), using a 785-nm laser line excitation and power of about 10 mW with 3 measurement repetitions of 30 s each. Micro-Raman was used because it provides information on both chemistry and structure of the samples under study.

The thermal decomposition temperature was determined using a melting point system Mettler Toledo MP90, operation time 10 s, heated from 50 to 400 °C. Experiments were carried out using two different heating rates: 5 and 10 °C min^{-1}.

Thermal analysis of copal and amber was performed with a STA 409C Netzsch equipment through simultaneous DTA-TG. Analyses were carried out in a dry nitrogen atmosphere with a constant flow ratio of 80 mL min^{-1}. Powdered samples of 20 mg were introduced in an alumina crucible and heated from 25 to 700 °C with a linear rate of 10 °C min^{-1}, followed by free cooling. Aluminium oxide PerkinElmer 0419-0197 is taken as reference.

HSM was used to visually characterize the morphological evolution of copal and amber as temperature increases from 25 to 1500 °C, with a heating ratio of 5 °C min^{-1} in air atmosphere. The test cylinders (~ 30 mm in diameter) were prepared by cold-pressed by means of powdered samples less than 45 μm in size and bounding them with a 1/20 solution of Elvacite® acetone in a uniaxial press.

Results and discussion

Colour

Copal specimens from Congo are translucent, 2–3 cm in diameter and cream to orange in colour (Fig. 1a). Baltic amber specimens with different characteristics were selected, one of them is yellow and transparent, another one is white-yellow and opaque, and the other is translucent and brownish. The Bitterfeld amber is slightly translucent and has a brownish colour (Fig. 1b, c).

The CIE $L*a*b*$ colour parameters for both copal and amber specimens are indicated in Table 1. Copal shows the most uniform colour values, while amber exhibits more variability (Fig. 2a). The resins lightness, L, increases proportionally to their chromatic parameter $b*$ (Fig. 2b). Copal exhibits intermediate L values in the range 48.34–53.51; the chromaticity is uniform, with $a* = 4.59–7.09$ and $b* = 7.60–13.72$, corresponding to the red–orange range. The colour saturation $C*$ ranges from 8.88 to 15.45, and the hue angle h ranges from 58.88 to 63.94.

In the case of amber, the yellow Yantarni sample has a contrastingly marked difference in colour parameters with respect to all of the other amber pieces. The lightness, L, of amber is in the range 45.39–48.07 except for the Yantarni specimen, with $L = 70.75$. The $a*$ parameter ranges from 0.89 to 5.99, and $b*$ is from 4.29 to 5.33. In the yellow Yantarni sample, $a*$ is 0.47 and $b*$ to 27.63. The C* parameter and h run from 4.38 to 8.01 and from 41.66 to 78.34, respectively; for the yellow Yantarni specimen $C*$ is 27.63; hue is 89.03. These parameters are important to investigate the original environmental conditions of the resins formation and also to know whether they have been treated to change

Fig. 1 Samples used in this study. **a** Congo copal, **b** amber from Bitterfeld, **c** amber from Yantarni
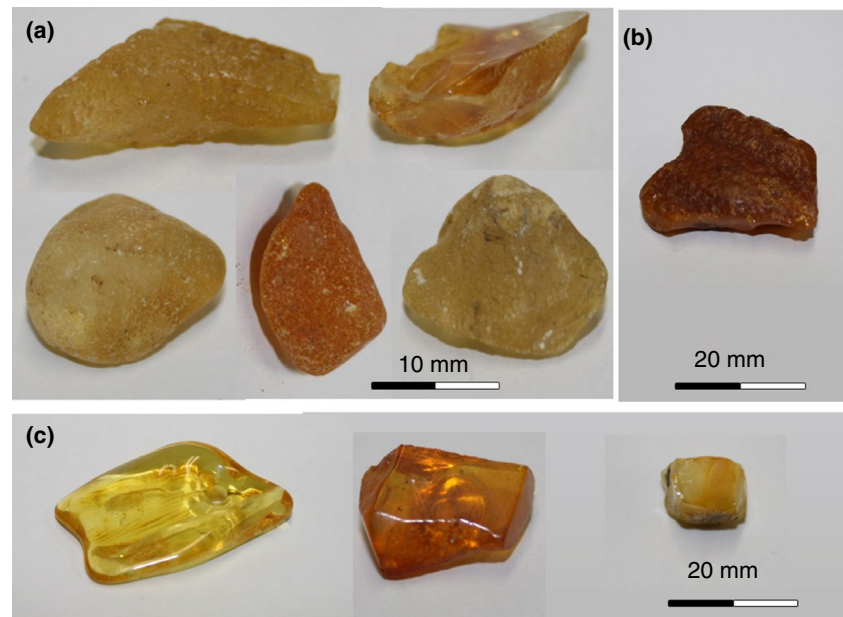
Table 1 Colour and CIELab parameters of the copal and amber specimens

Sample		L	a*	b*	C*	h	Δa*	Δb*	ΔL*	ΔE
Congo-1	Light yellow, translucent	53.51	7.09	13.72	15.45	62.68	7,19	13,83	-45.91	35.39
Congo-2	Dark yellow, translucent	48.34	4.59	7.60	8.88	58.88	4,68	7,71	-51.09	38.74
Congo-3	Yellow, translucent	50.70	5.26	9.83	11.15	61.87	5,35	9,94	-48.73	36.96
Congo-4	Yellow, translucent	49.54	4.87	9.95	11.07	63.94	4,96	10,06	-49.88	37.95
Congo-5	Light yellow, opaque	49.67	5.38	10.73	12.00	63.36	5,48	10,84	-49.75	38.01
Yantarni	Light yellow, opaque	45.39	0.89	4.29	4.38	78.34	7,45	12,65	-54.03	40.86
Yantarni	Yellow, transparent	70.75	0.47	27.63	27.63	89.03	0,99	4,40	-28.68	25.50
Yantarni	Honey yellow, transparent	46.80	5.99	5.33	8.01	41.66	0,58	27,73	-52.63	40.22
Bitterfeld	Yellow–brown, opaque	48.07	2.90	5.28	6.02	61.22	6,09	5,44	-51.36	38.54

Fig. 2 CIELab chromatic diagrams; **a** a^* vs b^* colour coordinates, **b** ΔL, lightness, vs Δb^* yellowing. HL, honey yellow; LY, light yellow; Y, yellow
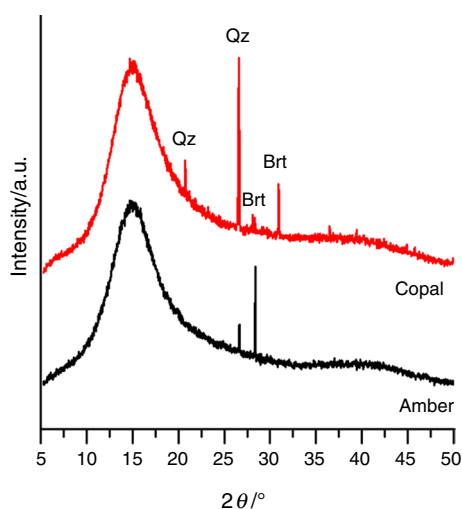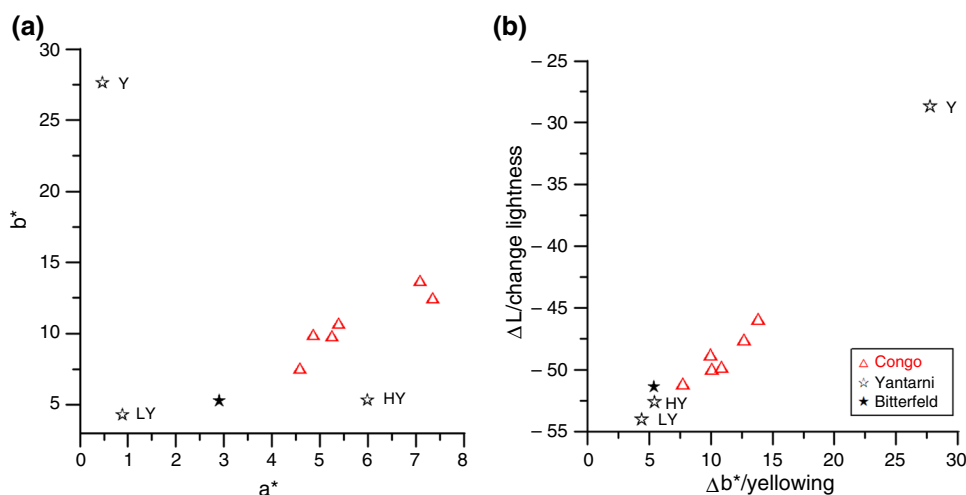
Fig. 3 XRD patterns from **a** Congo copal and **b** Baltic amber. Brt, barite; Qz, quartz

the colour to yellowing them. Presence of oxygen, pH, relative humidity are factors related to colour changes [22–24].

Mineralogical characterization

The XRD patterns show the amorphous state of the samples, characterized by a broad band centred at about 5.9 Å (~ 15°2θ), ranging from 10 to 25°2θ, typical of the majority of fossil resins (Fig. 3). In these samples, only traces of minerals were present, such as quartz (SiO_2) and barite ($BaSO_4$) in Congo copal.

SEM observations enabled to detect the presence of other minerals included in the amber samples (Fig. 4). Besides barite ($BaSO_4$), some pyrite (FeS_2) and gypsum ($CaSO_4 \cdot 2H_2O$) crystals were found in all of them. In the case of Bitterfeld amber, halite (NaCl) and silicates were

also found, which can be attributed to the class of phyllosilicates by their morphology. The presence of these mineral phases is relatively common in amber from different locations; for example, several authors [25, 26] found significant amounts of quartz in Baltic amber specimens. Quartz and calcite ($CaCO_3$) have also been reported [27]. These minerals occur as inclusions trapped within the copal and amber during their fossilization process, and they confer opacity to the specimens. In the case of transparent amber and copal, no significant mineral phases were observed. Another characteristic of amber is the presence of pores enclosed within its structure (Fig. 4d), which also induce opacity [28].

Molecular structure

FTIR analyses show differences between Congo copal and amber samples. The latter show typical FTIR fingerprints of Baltic amber pieces. Table 2 shows the results of amber and copal vibration bands compared with established by other authors, with their corresponding assignments [24, 26, 29–33]. The main differences between amber and copal are related to the presence/absence of bands at 3500–3400, 3095, 2362 cm^{-1} and around the 1245–1040 cm^{-1} range.

Representative FTIR spectra of amber and copal are shown in Fig. 5. They show two areas where copal and amber behave differently. The characteristic fingerprints of the Baltic amber are in the ranges 4000–2500 cm^{-1} and 1800–700 cm^{-1}. Nevertheless, Beck [29] suggested that the range of the spectrum from 1250 to 1100 cm^{-1}, corresponding to C–O stretching vibrations, is what defines whether an amber piece is from the Baltic region or not. Copal presents four frequencies with different intensity than amber at 3095, 1643, 1265 and the 887 cm^{-1}. These frequencies together with the Baltic shoulder allow to characterize or differentiate amber from copal. The 887 cm^{-1} band is also present
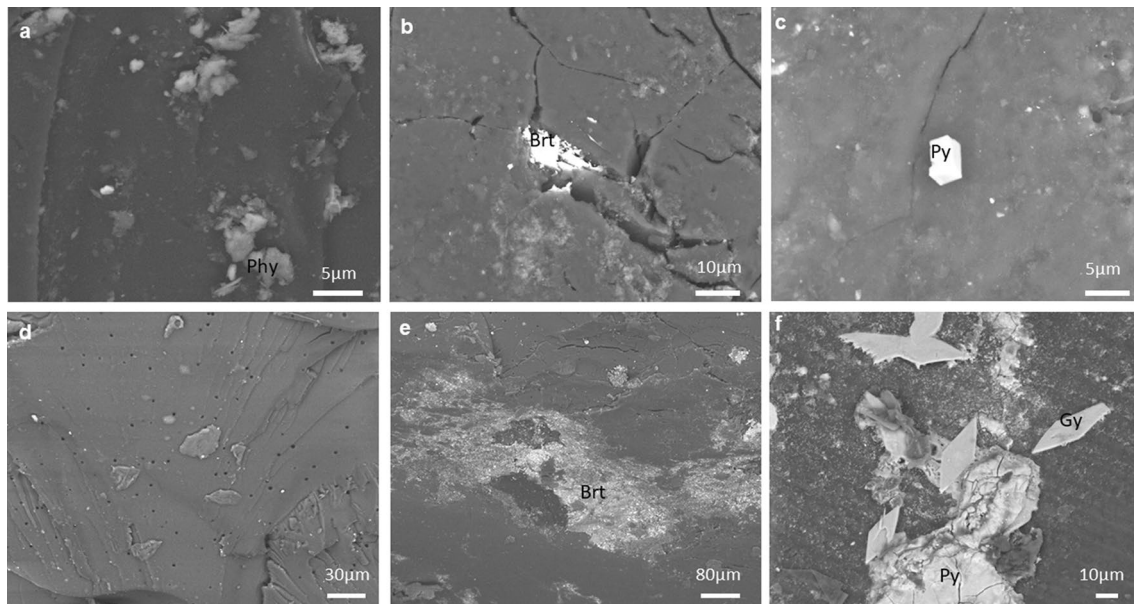
Fig. 4 SEM images of amber. **a**, **b**, **c** Bitterfeld specimens; **d**, **e**, **f** Yantarni amber

Table 2 FTIR bands, in wavenumbers/cm^{-1}, and vibrational assignments of the resin specimens (Yantarni: HL, honey yellow; LY, light yellow; Y, yellow). Assignments data from [24, 26, 29–33]

Bands/cm^{-1}	Yantarni HY	Yantarni LY	Yantarni	Bitterfeld	Copal	Assignment
$3500 - 3400$	3429	3369	3328	3327		O–H stretching, broad
3095	3095	3095	3095	3095	3095	C–H stretching
$2930 \pm 10/2853 \pm 10$	2924–2860	2925–2852	2926–2852	2926–2858	2927–2860	C–H stretching
2362 ± 5						C–O stretching (of succinate)
$1735 - 1700$	1735	1730	1735	1735–1700	1700	C=O stretching (carboxyl group)
$1650 - 1640$	1643	1640	1645	1644	1643	C=C stretching
1450 ± 20	1448	1455	1457	1445	1444	C–H bending
1375 ± 5	1374	1375	1375	1375	1385	C–H bending
$1245 - 1240/1262$					1265	C–O stretching
$1180 - 1160/1175$					1172	C–O stretching
1040					1040	C–O stretching
$1250 - 1010/1150 \pm 15$	1157	1157	1156	1154		C–O stretching (of succinite)
995 ± 15	982	996	992	979	979	C–H bending
888 ± 1	887	887	887	887	887	C–H bending

in amber, but it is appreciably smaller and decreases with oxidation; it can even disappear [34].

In the upper range of the spectrum, the amber samples show a broad absorbance shoulder around 3400 cm^{-1}, assigned to the O–H stretching bond of the hydroxyl group, possibly related to the water adsorbed during amber formation [32]. In copal, there is a sharp peak at 3095 cm^{-1}, attributed to the C–H stretching bond of the exocyclic C=CH$_2$ group, which is very weak in amber. In this study, this peak has been also observed in Baltic amber from Kaliningrad and also in the Bitterfeld specimens, but with a much lower peak intensity. A double C–H stretching vibration appears in the range 2926–2852 cm^{-1}, which corresponds to saturated bonds of methyl and methylene groups in amber. The 2362 cm^{-1} band is related to C–O vibrations in CO$_2$. The comparative FTIR results show some differences in the
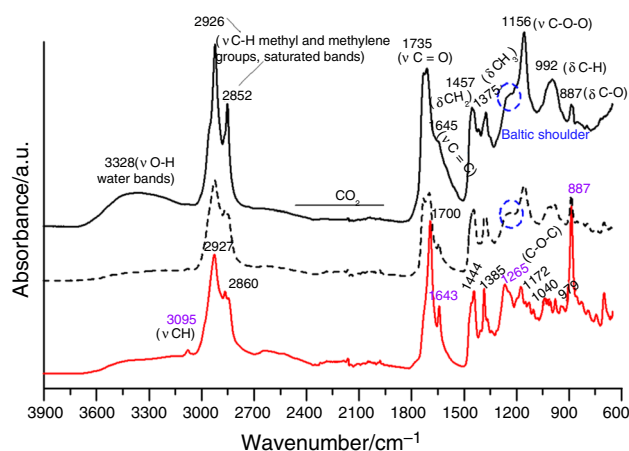
Fig. 5 FTIR spectra of a Congo copal (red) and Baltic amber (black) specimens, discontinuous line corresponds to Bitterfeld amber. Violet colour numbers show relevant peaks in copal, and the blue circle marks the typical Baltic shoulder

shape of the spectra (Fig. 5). The definition and intensity of the Bitterfeld amber are lower than those of the Yantarni amber. However, the fingerprint of Bitterfeld amber corresponds to the so-called Baltic shoulder.

The low FTIR range starts with pronounced intensity absorption peaks corresponding to the carboxyl group, C=O stretching, ranging from 1700 to 1735 cm^{-1} in amber samples, and attributed to the presence of acids and esters during ageing. These peaks may increase due to oxidation processes [32]. Copal shows only one peak at 1700 cm^{-1}. At ~ 1643 cm^{-1} amber shows a weak intensity peak, while copal exhibits a strong vibration, associated with C=C stretching attributed to RCH=CH$_2$, RR'C=CH$_2$ unsaturated compounds [31]. The intensity of this band is reduced with resins deterioration [32, 35]. The medium intensity absorption peaks around 1450 and 1380 cm^{-1} in both resins are

due to C–H bending vibrations and are related to methyl and methylene group (CH$_2$–CH$_3$).

In the amber samples a wide absorption shoulder in the region between 1255 and 1156 cm^{-1}, related to C–O stretching vibrations, is observed. This range is attributed to esters, alcohols and carboxylic acids, being this the typical Baltic shoulder. Succinate esters can be hydrolysed into communol and succinic acids; both of them are produced under wet and acidic conditions and are typical components of Baltic amber [24]. The slope of the Baltic shoulder may increase during amber degradation [29]. In this region, Congo copal shows three vibration bands around 1265, 1172 and 1040 cm^{-1}, due to C–O stretching [30, 36]. The last absorption peaks at 887 and 980 cm^{-1} are attributed to C–H bending. In copal they show stronger vibrations than to what is observed in amber [34, 37].

The main differences between Raman spectra of amber and copal are evidenced in the wavenumber regions from 2700 to 3200 cm^{-1} and from 600 to 1900 cm^{-1}, which are attributed to stretching vibrations of CH$_2$, CH$_3$ and CH$_2$, C=C, C=O, respectively (Table 3 and Fig. 6).

The Raman vibrational band around 1650 cm^{-1} is assigned to the stretching vibration of the olefinic group ν(C–CH$_2$) and the 1444 cm^{-1} band to the deformation of CH bonds (CH$_2$ or CH$_3$ groups). The triplet at 745, 718 and 697 cm^{-1} observed in the amber comes from the evolution of the doublet at 745 and 698 cm^{-1} in copal [4, 38, 39].

The polymerization degree or index of maturation L_m (maturity indicator level) is determined using the relative intensity ratio between two significant wavenumbers from mid-Raman spectrum: ν(C=C)/Δ (CH$_2$) = I^{1650}/I^{1445}. In amber samples, I^{1650}/I^{1453} is 0.9 and in copal I^{1699}/I^{1440} is 1.4, showing that this ratio decreases with resins maturity. In fact, the relative intensity ratio is consistently lower for amber (< 1) than for copal (> 1). These results are close to those of [36], who attribute the highest values to modern

Table 3 Assignments of Raman bands in the studied resins and wavenumber (cm^{-1}) of the spectra database

Reference	Bands/cm^{-1}	Amber	Copal	Vibrational assignment bands mode
	540		554	ν(COC) in-plane deformation
	651		641	ν(C–S) stretching
	881	881	882	ν(COC)
	938	938	948	ρ (CH$_3$)
	1298	1298	1286	Δ(CH$_2$) twisting
	1450	1453	1440	Δ(CH$_2$) deformation
[26]	1479		1475	Δ(CH$_2$), Δ (CH$_3$)
[4]	1646/1650	1650	1646	ν(C=C) stretching
[26]	1699		1699	ν(C=O)
	1734	1795	1795	ν(C–O) stretching ester
[4]	2871/2850	2870	2870	ν(CH$_3$) stretching
[4]	2930/2928	2928	2928	ν(CH$_2$) stretching
[4]	2965/3085		3020	ν(CH$_2$) stretching
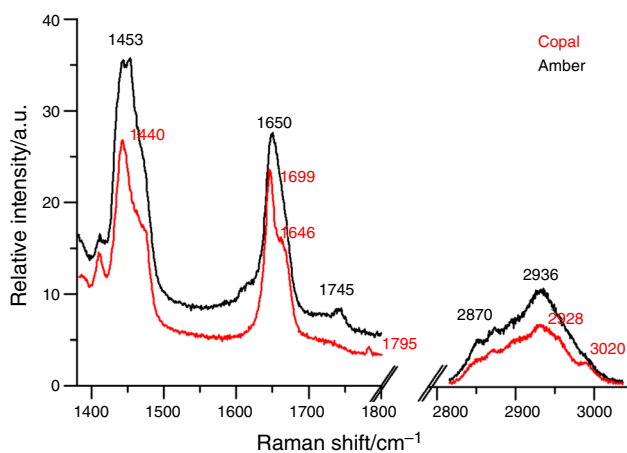
Fig. 6 Raman spectra of representative copal and amber samples with the vibrational wavenumbers of each band

Fig. 7 DTA curves corresponding to the analysed samples. Red line refers to copal and black line to amber (continuous line, Yantarni; dashed line, Bitterfeld). The temperature events are indicated in each case
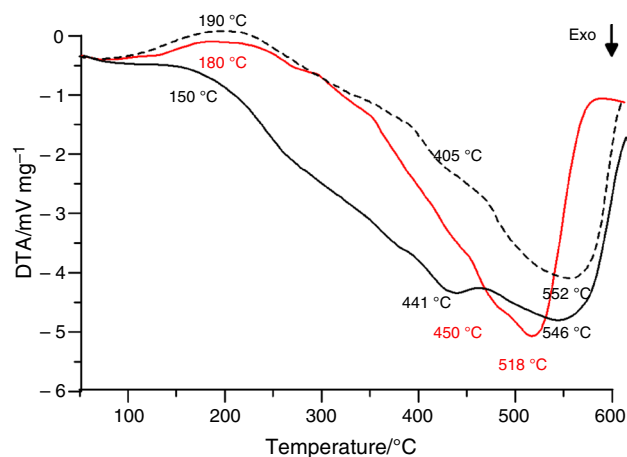
pine resins and the lowest to amber, due to the degradation of ν(C=C) attributed to meteorization or microbial oxidation.

In the upper region of the spectra, copal and amber vibration bands are similar. Nevertheless, the smooth peak at wavenumber 3020 cm^{-1}, corresponding to ν(CH), is only present in the copal samples. The strong peak around 2930 cm^{-1} is similar in amber and copal, but their intensity is different. In amber, peaks are centred at 2936 cm^{-1} and have an intensity of 9.5, while in copal, they are observed at 2928 cm^{-1} with a 6.5 intensity. Finally, the vibration at 2870 cm^{-1} shows a prominent shoulder in all cases.

Thermal behaviour

When the heating rate of the test is 10 °C min^{-1}, the decomposition temperature is not stable and varies within a range of about 35 °C, while tests carried out at a lower rate, 5 °C min^{-1}, provide similar decomposition temperature in all samples. In this last case, temperature values of about 165 °C and 385 °C are observed for copal and amber samples, respectively. The higher is the degree of polymerization of the resin, the higher its decomposition temperature.

DTA results show different behaviour between copal and amber. Yet, in all cases the observed events are broad and poorly defined (Fig. 7). According to [5], the curves present weak and unstructured phenomena that highlight the thermal behaviour of the resins. The first endothermic event is weak and wide, and it is observed between 150 and 190 °C, being attributed to evaporation processes [5]. When the temperature increases, a discrete and weak exothermic peak appears at 450 °C in copal specimens and a relatively pronounced exothermic process occurs at 518 °C. In amber, a weak exothermic event is evidenced at 405–441 °C. The most marked

exothermic peak occurs at 546 °C in the Yantarni specimens and at 552 °C in the Bitterfeld sample tested. These results indicate on one side the combustion of the resins and, on the other, the temperature increases with the resin polymerization degree. DTA results show peaks at higher temperatures than those reported for both copal and amber by other authors. Amber sample from Bitterfeld may show lower exothermic peaks, for example peaks at about 350 and 500 °C were reported by [7] that also observed lower exothermic peak temperatures for copal. The glass transition temperature (T_g) calculated from the DTA is 290 °C for copal and 386–387 °C for amber. These values are consistent with the maximal decomposition temperature in both types of resin. Other authors report lower T_g values, but they were calculated from the DSC analyses [8, 9, 40].

The main information about the thermal behaviour of resins can be obtained from TG and DTG. In this research, TG curves show that the decomposition of copal and amber starts above 225 °C and it is associated with the temperature at which a significant mass loss occurs (Fig. 8). Copal samples complete their combustion at around 550 °C, while amber samples at 600 °C. Congo copal lose its mass in two steps. Its maximum decomposition rate occurs in the range 225–440 °C when it loses in just one step 71 mass% of its initial mass. In the second step, at temperatures higher than 440 °C, copal loses the remaining 27 mass%. These two steps are correlated with two corresponding DTG peaks, the most intense of which occurs at 394 °C and the second smaller one at 507 °C (Fig. 9). In the Yantarni amber, the mass loss takes place in three stages. At temperatures in the range 225–380 °C, Yantarni amber loses 31 mass% of its initial mass, between 380 and 448 °C it loses 26 mass%, and from 448 to 600 °C, it loses the remaining 39 mass%.
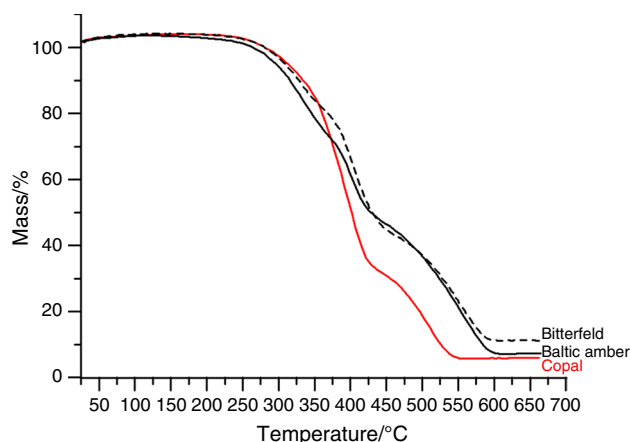
Fig. 8 Thermogravimetric analysis of Congo copal (red line), Yantarni amber (continuous line) and Bitterfeld amber (dashed line)
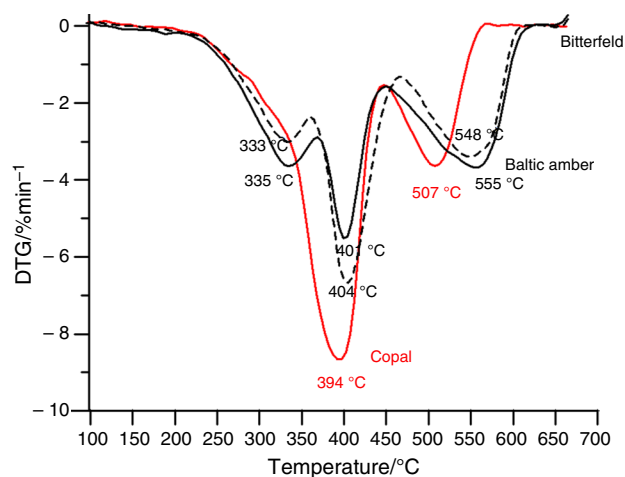
Fig. 9 Calculated DTG curves of Congo copal (red line), Yantarni amber (continuous line) and Bitterfeld amber (dashed line)

These stages are also associated with three DTG events, corresponding to a small peak at 335 °C, a big one at 401 °C and a medium one at 555 °C, respectively (Fig. 9). The Bitterfeld amber also loses its mass in three stages, at similar temperature ranges as those observed for Yantarni amber (Fig. 9). These losses are related not only to a release of water and other volatiles but also to the material degradation produced by heating in the absence of oxygen [33, 38].

These results show that amber has higher decomposition temperatures than copal. Some authors relate the temperature increase at the DTG peaks to the age of the fossil resin. This relationship may help to identify the origin of the resins and, at the same time, allows the determination of diagenetic processes [40–43].

Amber and copal have highly different rheological properties, as evidenced from the HSM results (Fig. 10). Congo copal exhibits a first shrinkage at 131 °C, which corresponds to the start of sintering (Fig. 10a). As temperature increases, it expands due both to material decomposition and generation of gases that cannot be released because of the copal plastic behaviour at these temperatures. The softening point occurs at 195 °C, and copal reaches the ball morphology at 215 °C. Finally, the increase in pressure produces an explosion, with an even lower viscosity of the liquid that can no longer support the internal pressure of gases, and the half ball morphology is attained at 395 °C.

The amber specimens maintain their viscosity up to a temperature of 150 °C (Fig. 10b). At this stage, the first shrinkage is observed and the softening temperature occurs at 450 °C. Up to a temperature of 540 °C, the specimen swells and the deformation process takes place. At 700 °C, amber attains its minimal viscosity and shrinkage occurs; above 700 °C, the sample morphology remains unchanged.

A summary of the main differential characteristics of studied copal and amber specimens is shown in Table 4.
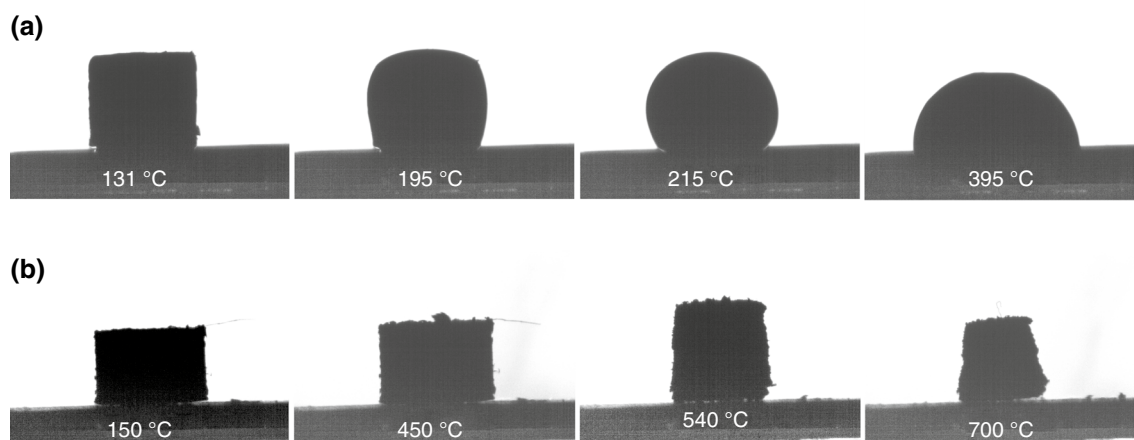
Fig. 10 Hot stage microscopy from **a** Congo copal and **b** Baltic amber

Table 4 Main differences between copal and amber in the analysed specimens

Samples	Copal	Bitterfeld	Baltic amber
Mineral inclusions	Quartz, barite, pyrite, gypsum, halite, phyllosilicates		
FTIR spectra/cm^{-1}	887	887 small	887 small
	1265, 1172, 1040	≈1255–1157 weak bands	≈1255–1157 Baltic shoulder
	3095 sharp peak	3095 weak band	3095 weak band
	Shoulder ≈ 3340 (oxidization)	Absent	≈3400 (OH-stretching)
Raman spectra/cm^{-1}	554, 641, 1475, 3020	745, 718, 697	
	2930 strong	2928 moderate	
Polymerization degree	I^{1699}/I^{1440} 1.4	I^{1650}/I^{1453} 0.9	
Thermal properties			
Decomposition/°C	165	385	
DTA exothermic/°C	150, 450, 518	190, 405, 552	180, 441, 546
TG/mass%	71 and 27	31, 32 and 29	31, 26 and 39
DTG peaks/°C	394, 507	333, 404, 548	335, 401, 555
Rheology/°C	Start sintering 131	Start sintering 150	
	Softening 195	Softening 450	
	Ball 215	Shrinkage 700	
	Half-ball 395		

Conclusions

Minerals and pore inclusions incorporated in the resins affect their colour and opacity. Usually, amber presents lower lightness and yellowing values compared to copal, with the exception of the yellow specimen from Yantarni.

FTIR and Raman spectroscopy show the degree of polymerization of the resins, which allows to classify them into copal or amber, according to the presence of different bands. All the FTIR spectra of amber include a broad, horizontal shoulder followed by a peak at 1157 cm^{-1} typically associated with Baltic amber (related to its succinite composition). Amber also exhibits a broad absorbance band around 3400 cm^{-1} related to water. This is more pronounced in the Yantarni amber. As would be expected, the I_m calculated from the Raman data is < 1 in amber, whereas it is > 1 in copal.

The thermal behaviour of copal and amber is related to their polymerization degree. The decomposition temperature of copal is about 165 °C, while it is 385 °C in amber. DTA shows two exothermic events, the first occurs at lower temperature in amber (from Bitterfeld and Yantarni) than in copal, whereas the second event takes place at lower temperatures in copal than in amber. The TG curves evidence the different thermal behaviour of the two resins, indicating the start of the decomposition processes at 225 and 440 °C copal and amber, respectively. The mass loss is complete at the end of the heating test, and it correlates with the peaks obtained from the DTG. Copal shows two peaks, while amber presents three peaks, two of them located at higher temperatures than in copal. This evolution is related to the polymerization degree.

The rheological properties of the resins have been revealed through HSM. Copal shows a more plastic behaviour than amber. As temperature increases, the morphology of copal specimens changes and it reaches to the half-ball shape at 215 °C. On the other hand, amber does not show a plastic behaviour with the increase of temperature; it just displays and only shows a small shrinkage at the end of the heating process.

References

1. Schlee D. Ungewöhnliche Farbvarianten des Baltische Bernsteins: blau, grau, orange und "gold" als Folge von Rissesystemen. In: Bernstein-Neiiigkeiten. Stuttgarter Beiträge zur Naturkunde, Series C vol 214(18); 1984. p. 2–98.

2. Grimaldi DA, Shedrinsky A, Ross A, Baer NS. Forgeries of fossils in "amber": history, identification and case studies. Curator: Museum J. 1994;37(4):251–74. https://doi.org/10.1111/j.2151-6952.1994.tb01023.x.

3. Lambert JB, Tsai CH, Shah MC, Hurtley AE, Santiago-Blay JA. Distinguishing amber and copal classes by proton magnetic resonance spectroscopy. Archaeometry. 2012;54(2):332–48. https://doi.org/10.1111/j.1475-4754.2011.00625.x.

4. Brody RH, Edwards HG, Pollard AM. A study of amber and copal samples using FT-Raman spectroscopy. Spectrochim Acta Part A: Mol Biomol Spectrosc. 2001;57(6):1325–38. https://doi.org/10.1016/S1386-1425(01)00387-0.

5. Feist M, Lamprecht I, Müller F. Thermal investigations of amber and copal. Thermochim Acta. 2007;458(1–2):162–70. https://doi.org/10.1016/j.tca.2007.01.029.

6. Pagacz J, Naglik B, Stach P, Drzewicz P, Natkaniec-Nowak L. Maturation process of natural resins recorded in their thermal properties. J Mater Sci. 2020;55(10):4504–23.

7. Cebulak S, Matuszewska A, Langier-Kuźniarowa A. Diversification of natural resins of various originoxyreactive thermal analysis and infrared spectroscopy. J Therm Anal Calorim. 2003;71(3):905–14.

8. Zhao J, Ragazzi E, McKenna GB. Something about amber: Fictive temperature and glass transition temperature of extremely old glasses from copal to Triassic amber. Polymer. 2013;54(26):7041–7. https://doi.org/10.1016/j.polymer.2013.10.046.

9. Jablonski P, Golloch A, Borchard W. DSC-measurements of amber and resin samples. Thermochim acta. 1999;333(1):87–93. https://doi.org/10.1016/S0040-6031(99)00101-X.

10. Wolfe AP, McKellar RC, Tappert R, Sodhi RN, Muehlenbachs K. Bitterfeld amber is not Baltic amber: three geochemical tests and further constraints on the botanical affinities of succinite. Rev Palaeobot Palyno. 2016;225:21–32. https://doi.org/10.1016/j.revpalbo.2015.11.002.

11. Sivkov VV, Zhamoida VA. Amber deposits in the Kaliningrad Region. In: Gritsenko VA, Sivkov VV, Yurov AV, Kostianoy AG, editors. Terrestrial and inland water environment of the Kaliningrad Region. Handb Environ Chem, vol. 65. Cham: Springer; 2018. p. 33–44.

12. Wolfe AP, Tappert R, Muehlenbachs K, Boudreau M, McKellar RC, Basinger JF, Garrett A. A new proposal concerning the botanical origin of Baltic amber. Proc Royal Soc B: Biol Sci. 2009;276(1672):3403–12. https://doi.org/10.1098/rspb.2009.0806.

13. Drzewicz P, Natkaniec-Nowak L, Czapla D. Analytical approaches for studies of fossil resins. TrAC Trends Anal Chem. 2016;85:75–84. https://doi.org/10.1016/j.trac.2016.06.022.

14. Dunlop A. Bitterfeld amber. In: Penny D, editor. Biodiversity of fossils in amber from the major world deposits. Manchester: Siri Scientific Press; 2010. p. 57–68.

15. Knuth G, Koch T, Rappsilber I, Volland L. Concerning amber in the Bitterfeld region geological and genetic aspects. Hallesches Jahrbuch für Geowissenschaften. 2002;24:35–46.

16. Sadowski EM, Schmidt AR, Seyfullah LJ, Solórzano-Kraemer MM, Neumann C, Perrichot V, Hamanna C, Milkef R, Nascimbene PC. Conservation, preparation and imaging of diverse ambers and their inclusions. Earth Sci Rev. 2021;220:103653. https://doi.org/10.1016/j.earscirev.2021.103653.

17. Yamamoto S, Otto A, Krumbiegel G, Simoneit BR. The natural product biomarkers in succinite, glessite and stantienite ambers from Bitterfeld. Germany Rev Palaeobot Palyno. 2006;140(1–2):27–49. https://doi.org/10.1016/j.revpalbo.2006.02.002.

18. Lambert JB, Nguyen TV, Levy AJ, Wu Y, Santiago-Blay JA. Structural changes from heating amber and copal as observed by nuclear magnetic resonance spectroscopy. Magn Reson Chem. 2020;58(9):812–9. https://doi.org/10.1002/mrc.4992.

19. Bouju V, Perrichot V. A review of amber and copal occurrences in Africa and their paleontological significance. Une révision des gisements d'ambre et de copal en Afrique et leur signification paléontologique. Bull Soc Géol Fr. 2020;191(1):17.

20. CIE. Technical report, colorimetry. Commission Internationale de L'Eclairage, 1931.

21. McGuire RG. Reporting of objective color measurements. Hort Science. 1992;27(12):1254–5.

22. Bisulca C, Nascimbene PC, Elkin L, Grimaldi DA. Variation in the deterioration of fossil resins and implications for the conservation of fossils in amber. Am Mus Novit. 2012;3734:1–19.

23. Pastorelli G. A comparative study by infrared spectroscopy and optical oxygen sensing to identify and quantify oxidation of Baltic amber in different ageing conditions. J Cult Herit. 2011;12(2):164–8.

24. Pastorelli G, Shashoua Y, Richter J. Hydrolysis of Baltic amber during thermal ageing—an infrared spectroscopic approach. Spectrochim Acta Part A: Mol Biomol Spectrosc. 2013;106:124–8.

25. Maliszewski K, Marciniak-Maliszewska BEATA, Kupryjanowicz J, Pielińska A. Gypsum crystals on surface of Baltic amber from beach findings. In: Proceedings of the International Amber Researcher Symposium 8, Warsaw 2013.

26. Pakutinskiene I, Kiuberis J, Bezdicka P, Senvaitiene J, Kareiva A. Analytical characterization of Baltic amber by FTIR, XRD and SEM. Can J Anal Sci Spectrosc. 2007;52(5):287–93.

27. Cruickshanka RD, Ko K. Geology of an amber locality in the Hukawng Valley, Northern Myanmar. J Asian Earth Sci. 2003;21:441–55.

28. Czechowski F, Simoneit BR, Sachanbiński M, Chojcan J, Wołowiec S. Physicochemical structural characterization of ambers from deposits in Poland. Appl Geochem. 1996;11(6):811–34.

29. Beck C, Wilbur E, Meret S, Kossove D, Kermani K. The infrared spectra of amber and the identification of Baltic amber. Archaeometry. 1965;8(1):96–109.

30. Martín Ramos P, Ruíz Potosme NM, Fernández Coppel IA, Martín Gil J. Potential of ATR-FTIR spectroscopy for the classification of natural resins. Biol Eng Med Sci Rep. 2018;4(1):3–6.

31. Wagner-Wysiecka E. Mid-infrared spectroscopy for characterization of Baltic amber (succinite). Spectrochim Acta Part A: Mol Biomol Spectrosc. 2018;196:418–31.

32. Pastorelli SP. Modeling of flexible components for studying a machining center control. Doctoral dissertation. Politecnico di Torino, 2019.

33. Zheng T, Li H, Lu T, Chen X, Li B, Liu Y. Spectroscopic identification of amber imitations: different pressure and temperature treatments of copal resins. Crystals. 2021;11(10):1223.

34. Guiliano M, Asia L, Onoratini G, Mille G. Applications of diamond crystal ATR FTIR spectroscopy to the characterization of ambers. Spectrochim Acta Part A: Mol Biomol Spectrosc. 2007;67(5):1407–11.

35. Shashoua Y, Degn Berthelsen MBL, Nielsen OF. Raman and ATR-FTIR spectroscopies applied to the conservation of archaeological Baltic amber. J Raman Spectrosc. 2006;37(10):1221–7.

36. Edwards HG, Farwell DW. Fourier transform-Raman spectroscopy of amber. Spectrochim Acta Part A: Mol Biomol Spectrosc. 1996;52(9):1119–25.

37. Delclòs X, Peñalver E, Ranaivosoa V, Solórzano-Kraemer MM. Unravelling the mystery of "Madagascar copal": age, origin and preservation of a Recent resin. PLoS ONE. 2020;15(5): e0232623.

38. Daher C, Paris C, Le Hô AS, Bellot-Gurlet L, Échard JP. A joint use of Raman and infrared spectroscopies for the identification of natural organic media used in ancient varnishes. J Raman Spectrosc. 2010;41(11):1494–9.

39. Badea GI, Caggiani MC, Colomban P, Mangone A, Teodor ED, Teodor ES, Radu GL. Fourier transform Raman and statistical analysis of thermally altered samples of amber. Appl Spectrosc. 2015;69(12):1457–63.

40. Pagacz J, Stach P, Natkaniec-Nowak L, Naglik B, Drzewicz P. Preliminary thermal characterization of natural resins from different botanical sources and geological environments. J Therm Anal Calorim. 2019;138(6):4279–88.

41. Ragazzi E, Roghi G, Giaretta A, Gianolla P. Classification of amber based on thermal analysis. Thermochim Acta. 2003;404(1–2):43–54.

42. Ragazzi E, Giaretta A, Perrichot V, Néraudeau D, Schmidt AR, Roghi G. Thermal analysis of *Cretaceous ambers* from southern France. Geodiversitas. 2009;31(1):163–75.

43. Giaretta M, Bianchin MD, Kanis LA, Contri RV, Külkamp-Guerreiro IC. Development of innovative polymer-based matricial nanostructures for Ritonavir oral administration. J Nanomater. 2019. https://doi.org/10.1155/2019/8619819.